

# Modelling the energy dependencies of high-frequency QPO in black hole X-ray binaries

Piotr T. Życki<sup>1\*</sup>, Andrzej Niedźwiecki<sup>2</sup> and Małgorzata A. Sobolewska<sup>3</sup>

<sup>1</sup>*Nicolaus Copernicus Astronomical Center, Bartycka 18, 00-716 Warsaw, Poland*

<sup>2</sup>*Łódź University, Department of Physics, Pomorska 149/153, 90-236 Łódź, Poland*

<sup>3</sup>*University of Durham, Physics Department, South Road DH1 3LE, UK*

Accepted 2007 April 24. Received 2007 April 13; in original form 2007 January 09

## ABSTRACT

We model energy dependencies of the quasi periodic oscillations (QPO) in the model of disc epicyclic motions, with X-ray modulation caused by varying relativistic effects. The model was proposed to explain the high frequency QPO observed in X-ray binaries. We consider two specific scenarios for the geometry of accretion flow and spectral formation. Firstly, a standard cold accretion disc with an active X-ray emitting corona is assumed to oscillate. Secondly, only a hot X-ray emitting accretion flow oscillates, while the cold disc is absent at the QPO radius. We find that the QPO spectra are generally similar to the spectrum of radiation emitted at the QPO radius, and they are broadened by the relativistic effects. In particular, the QPO spectrum contains the disc component in the oscillating disc with a corona scenario. We also review the available data on energy dependencies of high frequency QPO, and we point out that they appear to lack the disc component in their energy spectra. This would suggest the hot flow geometry in the spectral states when high frequency QPO are observed.

**Key words:** accretion, accretion disc – instabilities – relativity – X-rays: binaries – X-rays: individual: 4U 1630-47, GRO J1655-40, GRS 1915+105, XTE J1650-500, XTE J1550-564, H 1743-322

## 1 INTRODUCTION

High frequency (hecto-Hz) quasi-periodic oscillations are observed in X-ray power spectra of a number of black hole X-ray binaries. In some sources they occur in pairs, with frequency ratios close to 3:2 (see Remillard & McClintock 2006 for a recent review and Lachowicz, Czerny & Abramowicz 2006 for similar analysis of active galactic nuclei data). This latter property of the high- $f$  QPO (hfQPO hereafter) has stimulated development of a class of models, which interpret the QPO as a result of non-linear resonances (Kluźniak & Abramowicz 2001). Since the QPO frequencies are close to dynamical frequencies very near the central black hole, the models involve fast dynamical processes, for example epicyclic motions. In particular, resonances between the radial and vertical epicyclic motions have been considered by Abramowicz et al. (2003). Another suggestion was made by Blaes, Arras & Fragile (2006), who proposed the “breathing mode” (vertical pulsations) of a radiation pressure accretion disc in resonance with vertical epicyclic motion. The resonance condition  $\nu_\theta/\nu_r = 3/2$  then selects the radius where the oscillations are concentrated,  $r_{\text{QPO}}$ , and the observed modulation is produced. This radius has to be smaller than  $6GM/c^2$  to match the values of frequencies actually observed

in black hole binaries, indicating rotating black holes (e.g., Török et al. 2004).

The actual modulation of X-rays in the model of radial/vertical epicyclic motion resonances could be produced by variable relativistic effects, as the oscillating disk changes its position relative to unperturbed position (Bursa et al. 2004). These effects obviously affect only spectral components emitted at the QPO radius.

Generally, X-ray emission from accreting black holes consists of two main spectral components: thermal emission from the accretion disc and a component produced by inverse Compton up-scattering of a fraction of the disc photons in a hot plasma. In some sources a more complex spectra are also observed, e.g., with the disc component and two Comptonized components (e.g., Gierliński & Done 2003 and references therein). The reprocessed component (iron fluorescent  $K\alpha$  line and the Compton reflected continuum) are often present as well. The quasi-periodic X-ray modulation may then appear in all or only some of the components. Determining which components are actually modulated provides an important constraint on the model of the oscillations, since it constrains the physical process actually modulating the X-rays.

For example, energy dependencies of a related QPO phenomenon, the low-frequency QPO ( $f \lesssim 10$  Hz) in black hole binaries, reveal that it is the Comptonized component that is modulated (Sobolewska & Życki 2006). The disc component does not par-

\* e-mail: ptz@camk.edu.pl

ticipate in the modulation. Moreover, the QPO spectrum is harder than the time averaged spectrum (at least in the soft spectral states), consistent with the QPO being driven by modulations of the heating rate of the comptonizing plasma. This has an important consequence in that any model postulating disc origin of the oscillations must provide a mechanism of transferring the oscillations to the hot Comptonizing plasma without affecting the disc emission (Życki & Sobolewska 2005).

In this paper we attempt to make a first step towards similar analysis of the hfQPO. First, we review the available data on energy dependencies of the hfQPO. We then simulate the dependencies for the specific hfQPO model of resonant epicyclic motions, with X-ray modulations solely due to varying relativistic effects.

We consider two specific geometrical models. In the first model the standard accretion disc is envisioned to extend all the way to the last stable orbit and the hard X-rays are produced in a hot corona extending above the disc. As a consequence, three spectral components are produced at the QPO radius: thermal disc emission, hard Comptonized component and the reprocessed component. We will also extend this model to include an additional optically thick Comptonized component emitted at the QPO radius. This is motivated by results of more careful analyses of spectra and energetics of very high state showing such additional component (e.g., Done & Kubota 2006 and references therein). In this scenario we assume that both the disc and the corona undergo epicyclic oscillations, so the relativistic effects affect all spectral components.

In the second model, the standard disc is truncated somewhere above  $r_{\text{QPO}}$  and replaced by an inner hot flow. Thus, only the hot plasma undergoes epicyclic oscillations, while the disc flux is not subject to those motions. Only the Comptonized component is thus produced at  $r_{\text{QPO}}$ , and it is modulated by the relativistic effects.

## 2 OBSERVATIONAL DATA OF HIGH FREQUENCY QPO

To date there are seven X-ray black hole binaries with power spectra that show high-frequency ( $\gtrsim 100$  Hz) QPO. Usually, these fast QPO are detected in the hard energy band and are less significant in the soft energy band (e.g. 4U 1630-47: Klein-Wolt, Homan & van der Klis 2004; GRS 1915+105: Belloni et al. 2006). For instance, in XTE J1859+226 oscillations with frequencies of 150 and 187 Hz were found in the 5.9–60 keV band, while in the 2–5.9 keV band neither of the QPO yielded a significant detection (Cui et al. 2000). In XTE J1650-500 the 250 Hz QPO is detected with rms amplitude of  $< 0.85$  per cent, 4.5 per cent, and  $< 12.1$  per cent in the 2–6.2, 6.2–15.0 and 15.0–60.0 keV bands, respectively (Homan et al. 2003). In XTE J1550-564 the 185 Hz QPO is found with rms amplitude significantly higher in the 6–12 keV band than in the 2–6 keV band (Remillard et al. 1999a; see also Miller et al. 2001 and Homan et al. 2001). In GRO J1655-40 the 450 Hz QPO shows an increase of the rms amplitude from  $< 0.4$  per cent in the 2–12 keV band to 4.8 per cent in the 13–24 keV band (Strohmayer 2001a). In H 1743-322 the 160 and 240 Hz QPO have rms increasing from  $< 0.6$  per cent ( $< 1.2$  per cent) in the 3.3–5.8 keV band to 2.3 per cent (1.3 per cent) in the 5.8–20.9 keV band for upper (lower) QPO and both QPO have rms amplitude  $< 13$  per cent in the 21–60 keV band (Homan et al. 2005; see also Remillard et al. 2006). The 67 Hz QPO in GRS 1915+105 has the rms amplitude increasing from 1.5 per cent below 5 keV to 6 per cent above 13 keV (Morgan, Remillard & Greiner 1997; Cui 1999). To illustrate the trends in energy we plot in Fig. 1 the high- $f$  power spectra of GRS 1915+105 data analyzed in Strohmayer (2001b).

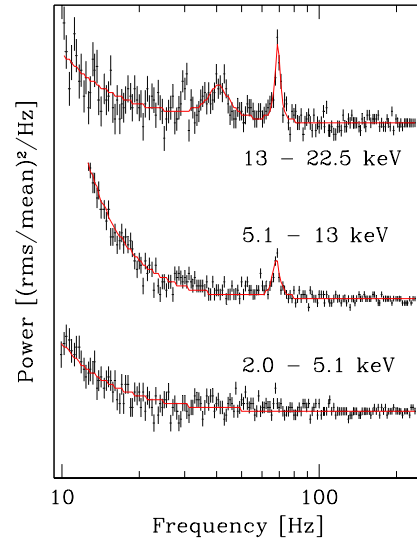


**Figure 1.** High- $f$  part of power spectrum of GRS 1915+105 in three energy bands (white noise was not subtracted and the spectra were shifted with respect to each other for a better comparison). In the softest energy band the high- $f$  QPO at 67 Hz is undetectable. It appears in the intermediate energy band with rms of 0.9 per cent. In the hardest energy band the rms of the QPO increases to 3.5 per cent. In addition, another 42 Hz QPO appears. The frequencies of these two QPO are in a ratio close to 3:2.

There are however observations that contradict this general trend. For example, the slightly slower 65 Hz QPO discovered in XTE J1550-564 shows very clear decrease of the rms amplitude with energy (5.5 per cent in the 2–6 keV band, 4.7 per cent in the 6–15 keV band, and  $< 4.5$  per cent in the 15–67 keV band; Kalemci et al. 2001). We note though that this QPO was discovered during a transition to the hard state, while the other hfQPO are typically seen in the very high state. Another interesting example is that of GRO J1655-40. While the 450 Hz QPO shows the typical increase in the rms amplitude as mentioned above, the 300 Hz QPO is seen *only* in the soft, 2–12 keV, band with typical rms amplitude of 0.8 per cent (Remillard et al. 1999b; Strohmayer 2001a). This could mean that the 300 Hz QPO has a different energy dependence and its rms decreases with energy. Another possibility is that the rms is simply too low to be detectable in the hard band, where photon statistics is worse. This was pointed out by Strohmayer (2001a) who place the upper limit on the QPO rms amplitude in the 13–24 keV band at 1.7 per cent.

The interesting phenomenon of double hfQPO with integral frequency ratios of 2:3 or 3:5 was observed in a few sources. These include the 300 and 450 Hz QPO in GRO J1655-40 (Remillard et al. 1999b, 2002; Strohmayer 2001a), 160 and 240 Hz QPO in H 1743-322 (Homan et al. 2005; Remillard et al. 2006), 150 and 187 Hz QPO in XTE J1859+226 (Cui et al. 2000), or somewhat lower frequency, 41 and 67 Hz, QPO in GRS 1915+105 (Morgan et al. 1997; Strohmayer 2001b). However, these pairs of QPO are not always detected simultaneously. Moreover, due to limited statistics it is not always apparent whether this is a pair of QPO, or one QPO moving in frequency (e.g. Miller et al. 2001; Homan et al. 2003). The best example here may be XTE J1550-564 for which the hfQPO were observed in a wide frequency range, 100–285 Hz (e.g. Homan et al. 2001). However, Remillard et al. (2002) show that frequencies of these QPO cluster preferentially around 184 and 276 Hz.

### 3 THE MODEL

We adopt the standard description of overall X-ray emission from X-ray binaries, that the thermal emission comes from an optically thick accretion disc, and the disc photons can be Comptonized in a hot plasma forming the hard emission component. The hard X-rays can be further reprocessed in the accretion disc. Our basic assumption is that there is no specific quasi-periodic modulation of the intrinsic emission, and the observed QPO is a result of relativistic effects (although the intrinsic emission can be randomly variable producing the usual broad band power spectrum). We consider two geometrical scenarios: an accretion disc extending to the last stable orbit with a hot active corona above it, and an accretion disc replaced by a hot flow inside certain radius, somewhat larger than the QPO radius.

Emission from the optically thick accretion disc is described by the standard disc black body approximation with temperature varying with radius as,

$$T(r) = T_0 F(r)^{1/4}, \quad (1)$$

where  $F(r)$  (assumed normalized to unity at its maximum) describes the radiation flux due to gravitational energy dissipation, as a function of radius for a given angular momentum of the black hole (see Krolik 1999, p. 150). The Comptonized component is computed using the THCOMP code of Zdziarski, Johnson & Magdziarz (1996). This is parameterized by the asymptotic slope of the spectrum,  $\Gamma$ , plasma optical depth,  $\tau_T$ , and seed photon temperature  $T_s$ . We assume that hot plasma properties do not depend on the radius, and we adopt  $\Gamma = 2.25$ ,  $\tau_T = 0.1$ . Obviously,  $T_s = T(r)$ . The reprocessed component is represented here by the Fe K $\alpha$  line emitted at 6.4 keV, with equivalent width of 100 eV.

For photon transfer we consider a Kerr black hole characterized by its mass,  $M$ , and angular momentum,  $J$ . We use the Boyer-Lindquist coordinate system  $(t, R, \theta, \phi)$ . The following dimensionless parameters are used below

$$r = \frac{R}{R_g}, \quad \hat{t} = \frac{ct}{R_g}, \quad a = \frac{J}{cR_g M}, \quad \Omega = \frac{d\phi}{dt}, \quad (2)$$

$$\Delta = r^2 - 2r + a^2 \quad (3)$$

$$\Sigma = r^2 + a^2 \cos^2 \theta \quad (4)$$

$$A = (r^2 + a^2)^2 - a^2 \Delta \sin^2 \theta, \quad (5)$$

where  $R_g = GM/c^2$  is the gravitational radius.

We assume that a disc element oscillates vertically and radially with respect to an equilibrium circular orbit

$$r(\hat{t}) = r_0 + r_{\max} \cos(\Omega_r \hat{t}) \quad (6)$$

$$\theta(\hat{t}) = \theta_0 + \frac{r_{\max}}{r_0} \cos(\Omega_\theta \hat{t}) \quad (7)$$

where  $\Omega_\theta$  and  $\Omega_r$  are vertical and radial epicyclic frequencies observed at infinity:

$$\Omega_\theta^2 = \Omega_K^2 (1 - 4ar^{-3/2} + 3a^2 r^{-2}) \quad (8)$$

$$\Omega_r^2 = \Omega_K^2 (1 - 6r^{-1} + 8ar^{-3/2} - 3a^2 r^{-2}), \quad (9)$$

$\Omega_K$  is the Keplerian angular velocity

$$\Omega_K = \frac{1}{r^{3/2} + a}. \quad (10)$$

The equilibrium position corresponds to  $\theta_0 = \pi/2$  and  $r_0$  given by the resonance condition  $\Omega_\theta/\Omega_r = 3/2$ . This gives  $r_0 = 3.9$  for  $a = 0.998$  and  $r_0 = 10.8$  for  $a = 0$ . In our simulations we assume  $r_{\max} = 0.1r_0$ . Note that we assume that  $r(\hat{t})$  and  $\theta(\hat{t})$  do

not depend on the azimuthal angle, which means that the whole ring oscillates in phase.

We construct the transfer function following a Monte Carlo method described in detail in Życki & Niedźwiecki (2005), modified to implement the source motion corresponding to oscillations. A large number of photons are emitted from consecutive positions of the source,  $r_i = r(\hat{t}_i)$  and  $\theta_i = \theta(\hat{t}_i)$  given by equations (6) and (7), with the phase of oscillations parameterized by  $\hat{t}_i$ . The initial azimuthal angle in the source rest frame,  $\phi_{\text{em}}$ , is generated from the uniform distribution. The polar angle between the photon initial direction and the vertical direction,  $\theta_{\text{em}}$ , is used as a parameter for the transfer function. Solving equations of photon motion, as described below, we find the energy shift ( $g = E_{\text{inf}}/E_{\text{rest}}$ ;  $E_{\text{inf}}$  and  $E_{\text{rest}}$  is the photon energy at infinity and in the source rest frame, respectively), inclination and arrival time,  $(g, i, \Delta\hat{t})$ . Each element of the transfer function,  $\mathcal{T}(\hat{t}_i, i, g, \Delta\hat{t}, \theta_{\text{em}})$ , is computed by summing all photon trajectories emitted from  $(\theta_i, r_i)$  for all angles,  $\phi_{\text{em}}$ , for which required  $(g, i, \Delta\hat{t})$  are obtained.

The travel time and the change of azimuthal angle of a photon emitted at  $(\theta_i, r_i)$  are given by

$$\Delta\phi_{\text{ph}} = \int_{\theta_i}^i \frac{\lambda - a \sin^2 \theta}{\Theta^{1/2} \sin^2 \theta} d\theta + \int_{r_i}^D \frac{a(r^2 + a^2 - \lambda a)}{\Delta \Re^{1/2}} dr, \quad (11)$$

$$\Delta\hat{t}_{\text{ph}} = \int_{\theta_i}^i \frac{a(\lambda - a \sin^2 \theta)}{\Theta^{1/2}} d\theta + \int_{r_i}^D \frac{(r^2 + a^2)(r^2 + a^2 - \lambda a)}{\Delta \Re^{1/2}} dr, \quad (12)$$

where  $\Re$  and  $\Theta$  are radial and polar effective potentials, respectively,

$$\Re(r) = (r^2 + a^2 - \lambda a)^2 - \Delta [\eta + (\lambda - a)^2],$$

$$\Theta(\theta) = \eta + \cos^2 \theta (a^2 - \lambda^2 / \sin^2 \theta), \quad (13)$$

$\eta$  and  $\lambda$  are photon constants of motion,

$$\eta \equiv \frac{Qc^2}{E_{\text{inf}}^2 R_g^2}, \quad \lambda \equiv \frac{Lc}{E_{\text{inf}} R_g}, \quad (14)$$

$Q$  is the Carter's constant and  $L$  is the component of angular momentum parallel to the black hole rotation axis. The angle,  $i$ , at which the photon is observed far from the source is determined by the integral equation of motion

$$\int_{r_i}^D \Re^{-1/2} dr = \int_{\theta_i}^i \Theta^{-1/2} d\theta. \quad (15)$$

Photon momentum components in the source rest frame are related to the emission angles,  $p_\theta = E_{\text{rest}} \cos \theta_{\text{em}}$ ,  $p_\phi = E_{\text{rest}} \sin \theta_{\text{em}} \sin \phi_{\text{em}}$ ,  $p_r = E_{\text{rest}} \sin \theta_{\text{em}} \cos \phi_{\text{em}}$ . Performing two subsequent Lorentz transformations, first from the source rest frame to the rest frame of a Keplerian observer, with the relative velocity

$$v^r = -r_{\max} \Omega_{(r)} \sin(\Omega_r \hat{t}_i) \quad (16)$$

$$v^\theta = -r_{\max} \Omega_{(\theta)} \sin(\Omega_\theta \hat{t}_i) \quad (17)$$

$$v^\phi = 0, \quad (18)$$

where

$$\Omega_{(\theta)} = \Omega_\theta (d\tau/dt)^{-1} \quad \Omega_{(r)} = \Omega_r (d\tau/dt)^{-1} \quad (19)$$

and  $d\tau/dt$  is the time dilation factor

$$\frac{d\tau}{dt} = r \left( \frac{\Delta}{A} \right)^{1/2} (1 - V^2)^{1/2}, \quad (20)$$

and the second transformation to the locally non-rotating frame (see Bardeen, Press & Teukolsky 1972), with the relative (Keplerian) velocity

$$V = (\Omega_K - 2ar/A) \frac{A}{r^2 \Delta^{1/2}}, \quad (21)$$

we find photon energy  $E_{\text{in}}$  and momentum  $(p_{(r)}, p_{(\theta)}, p_{(\phi)})$  in the locally non-rotating frame. Then, photon energy at infinity and constants of motion are given by [see eqs. (10) in Niedźwiecki (2005)]

$$E_{\text{inf}} = \left( \frac{\Delta \Sigma}{A} \right)^{1/2} E_{\text{in}} + \frac{2ar \sin \theta}{(A \Sigma)^{1/2}} p_{(\phi)} \quad (22)$$

$$\lambda = A \left( \frac{E_{\text{in}} \Sigma \Delta^{1/2}}{p_{(\phi)} \sin \theta} + 2ar \right)^{-1} \quad (23)$$

$$\eta = \Sigma \frac{p_{(\theta)}^2}{E_{\text{inf}}^2} + \cos^2 \theta \left( \frac{p_{(\phi)}^2}{E_{\text{inf}}^2} \frac{A}{\Sigma} - a^2 \right). \quad (24)$$

The transfer function was computed for three periods of the  $\theta$ -oscillation,  $P_\theta = 2\pi/\Omega_\theta$ ,  $T = 3P_\theta = 2P_r$ , with the total time  $T$  divided into  $N = 216$  time intervals. Obviously, the transfer function is periodic, with period  $T$ . The oscillations were followed for a number of  $T$  intervals, so that the QPO frequencies are better resolved in PDS, and we have checked that the final QPO spectra do not depend on the number of  $T$  intervals used. For the spectral computations presented we simulate the oscillations for total time  $16T$ . The time step in the simulations is equal to the time interval between the consecutive transfer functions,  $T/N$ . The middle position of the ring is computed at each time point when a transfer function is known,  $t_i$  (modulo  $T$ ), and it is given by  $r(t_i)$  and  $\theta(t_i)$  according to equations (6) and (7). For each  $t_i$  the energy spectrum of radiation emitted at  $r_{\text{QPO}}$  is convolved with the transfer function producing a signal observed at infinity.

The sequence of spectra created by the above procedure is subject to standard analysis in the time and Fourier domains (Życki 2003 and references therein). Power spectra are computed in each energy channel. These consist of a number of narrow peaks, since the lightcurves are strictly periodic. We compute the rms variability (normalized to the mean) integrating each peak over frequency, in each energy channel. This, multiplied by the time average energy spectrum gives the QPO energy spectrum (Życki & Sobolewska 2005). Note, that because of arbitrary values of epicyclic motion amplitude and a schematic geometry, the rms amplitude of the model QPO does not have a physical meaning. The purpose of this paper is to study the shape of the QPO energy spectra.

## 4 RESULTS

We note first that under the influence of relativistic effects the shape of a simple power law spectrum does not change. In the context of our models this means that a QPO energy spectrum would be the same as the input power law spectrum. However, X-ray spectra of X-ray binaries are not simple power laws. Moreover, the modulation affects only a fraction of emission originating around the resonance radius, and we can also expect discrete spectral features (the Fe  $K\alpha$  line) to be distorted by these effects. Thus, the QPO spectrum can be expected to be different than the time average spectrum, giving a potential diagnostic of the QPO model.

We first discuss the geometry of a disk extending to the marginally stable orbit, with the hard X-rays produced in a corona extending over a range of radii and X-ray reprocessing taking place locally. We assume that both the disc and the corona undergo

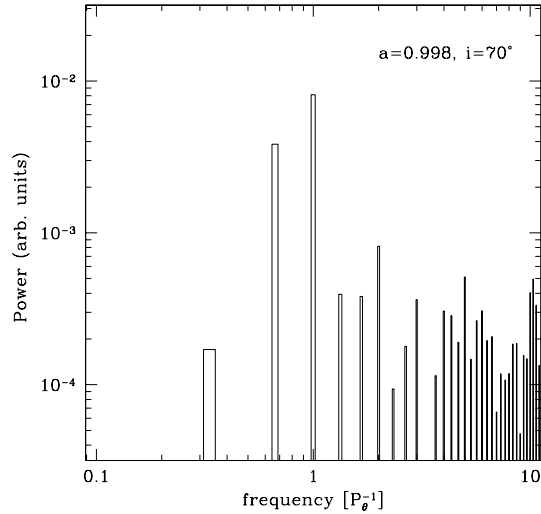


**Figure 2.** Power spectra from the model with maximally rotating,  $a = 0.998$ , Kerr black hole, for a source inclined at  $i = 70^\circ$ . The two main peaks correspond to  $f = 2/3$  and  $1 \times P_\theta^{-1}$  oscillations. Sub(harmonics) are present but are much weaker than the main peaks. The relative strength of the two oscillations is not a robust prediction of the model since it depends on the relative amplitudes of the  $\theta$  and  $r$  oscillations. These can only be predicted by a self-consistent dynamical simulations.

epicyclic oscillations and, in consequence, the relativistic effects from the deformed precessing ring affect all three spectral components. Thus, all three components can be expected to appear in the QPO spectrum. Power spectrum from the light curve at 10 keV, for a maximally rotating black hole with  $a = 0.998$  and a high inclination of  $i = 70^\circ$ , is plotted in Fig. 2. It shows the two main QPO peaks, at  $f = 2/3$  and  $1 P_\theta^{-1}$ , as well as many other (sub)harmonics. Relative height of the two main peak is not a robust prediction of the model, since it depends on the (arbitrary) oscillation amplitudes of the two epicyclic motions. We note that the other peaks are much weaker than the two main QPOs, and therefore would be impossible to detect in current data.

The QPO spectra for  $f = 2/3, 1$  and  $2 P_\theta^{-1}$  are plotted in Fig. 3a, together with the time average spectra for comparison. The QPO spectra do indeed contain both the disc component and the Fe  $K\alpha$  line. The disc component in the strongest,  $f = 1$ , QPO is rather narrow and significantly blueshifted. The disc component in the weaker,  $f = 2/3$ , QPO is somewhat broader, and less strongly blueshifted. In the weak  $f = 2$  QPO the disc component is not really distinctly visible and the low energy cutoff is rather broad. The positions of the Fe  $K\alpha$  line give us a clue to the behaviour of the disc component. In all QPO spectra there is a line component around  $E \approx 8.3$  keV, which is the line energy blueshifted by the maximum blueshift,  $g_{\text{max}}$  for the considered set of parameters:  $a$ ,  $r_{\text{QPO}}$  and  $i$ . In the  $f = 2/3$  and  $f = 2$  QPOs there are also weak structures around  $E \approx 2.2$  keV, corresponding to the maximum redshift,  $g_{\text{min}}$ . Values of these extreme shifts vary as a result of disc precession, and this causes the observed disc emission to vary. It is the variable spectrum that appears as the QPO spectrum. The variability is strongest near the extreme energy shifts, and therefore discrete spectral features in the QPO spectra are mainly located at those extreme positions. Differences between spectra at different  $f$  result from different behaviour of the extreme energy shifts when

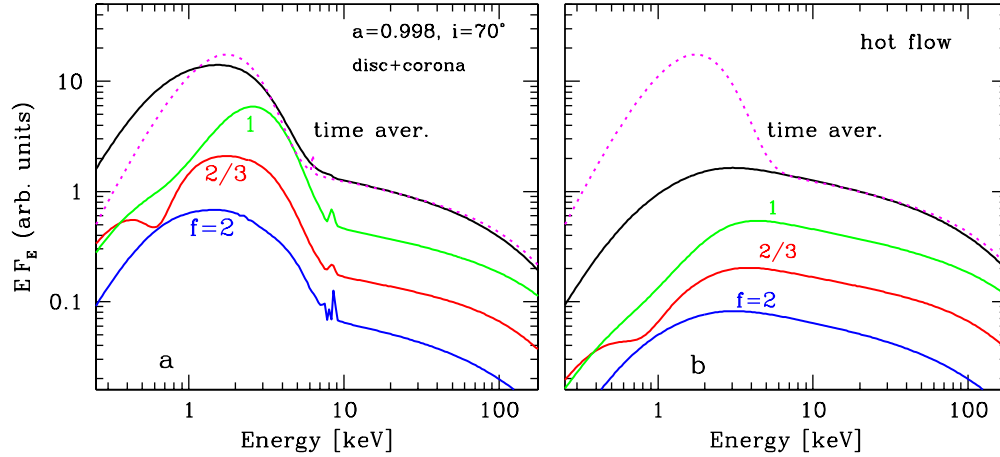


**Figure 3.** The QPO spectra for a maximally rotating black hole case, for inclination of  $70^\circ$ . The upper thick solid curve (black) is the time average spectrum of the time dependent component of radiation emitted at  $r_{\text{QPO}}$  (thus it does not contain the constant disc component in the hot flow geometry in b). The dotted curve (magenta online) is the spectrum from  $r_{\text{QPO}}$  but without the relativistic effects. The three curves labeled  $f = 2, 2/3, 1$  (blue, red, green online) show the QPO spectra for given  $f$  in units of  $1/P_\theta$ , i.e. the inverse of oscillation period in the  $\theta$ -coordinate. Left plot (a) shows the spectra for disc with a corona geometry, where the relativistic effects affect all spectral components (disc emission, Comptonization and the Fe  $K\alpha$  line), while plot (b) shows results for the inner hot flow geometry, where only the Comptonized emission is modulated. Normalizations of the spectra are arbitrary, but the order of the QPO curves corresponds to the strength of the QPO.

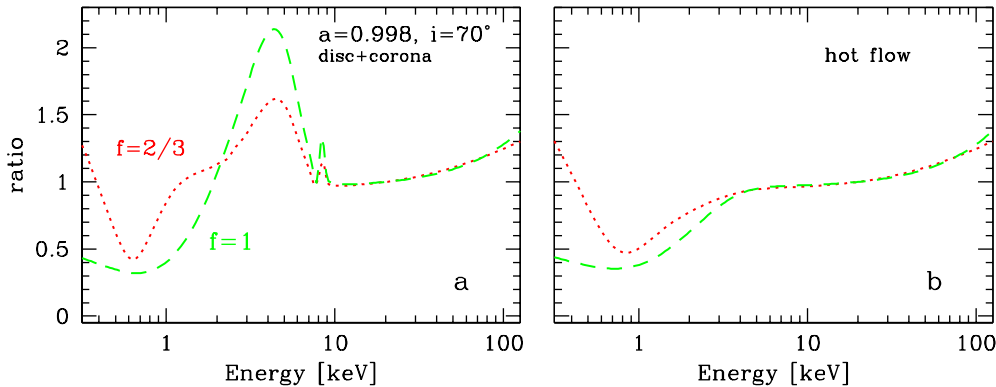


**Figure 4.** Ratios of the QPO spectra for  $a = 0.998$  and  $i = 70^\circ$  to the time averaged spectra from  $r_{\text{QPO}}$  in the disc with a corona geometry (a) and the hot flow geometry (b). The QPO spectra are practically identical to the time averaged spectra above 10 keV. Below that, in the disc plus corona geometry the QPO spectra show features related to Fe  $K\alpha$  line variability, while in hot flow geometry QPO spectra show stronger cutoff compared to the time averaged spectra (see also Fig. 3).

folded (observed) at different sub-periods ( $1P_\theta$  and  $P_r = 3/2P_\theta$ ) of the total period,  $3P_\theta$ .

The QPO spectra in the geometry of inner hot flow are plotted in Fig. 3b, for the same  $a$  and  $i$ , for direct comparison. Here, only the Comptonized component is variable, so neither the disc nor the Fe line are visible in the QPO spectra. The spectra are featureless and the only difference between different  $f$ 's is in the low energy cutoff, again related to different behaviour of energy shifts at different periods.

Fig. 4 shows ratios of the QPO spectra to the time averaged spectrum, for  $a = 1$  and  $i = 70^\circ$ , to demonstrate better the differences between them. The QPO spectra are different from the mean spectra only below  $\approx 10$  keV. In the disc plus corona geometry they show spectral features related to the variability of the Fe  $K\alpha$

line, as discussed above. In the hot flow geometry the QPO spectra show stronger cutoffs around 10 keV, clearly visible in the ratio representation.

The strength of relativistic distortions depends on the inclination angle of the source, therefore we show in Fig. 5 similar spectra for an inclination of  $i = 30^\circ$  and  $a = 0.998$ . For the lower  $i$  the range of redshift attained is narrower than for a higher  $i$ , and  $g_{\text{max}} < 1$ , due to strong gravitational redshift. As a result, the QPO spectra contain a distinct black body component (it is less smeared than in the previous case), while the blue component of the Fe  $K\alpha$  line is at lower energy than it is in the time averaged spectra. The QPO spectra from the hot flow geometry are again featureless, and the low-energy cutoffs are somewhat sharper than in the high- $i$  case, due to narrower range of energy shifts.

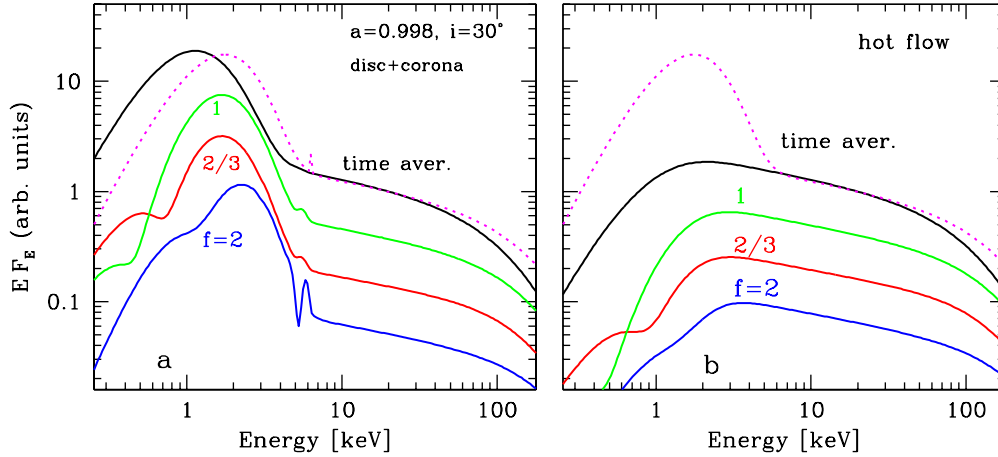


**Figure 5.** The QPO spectra for a maximally rotating black hole case, for inclination of  $30^\circ$ . The curves are labeled as in Fig. 3.

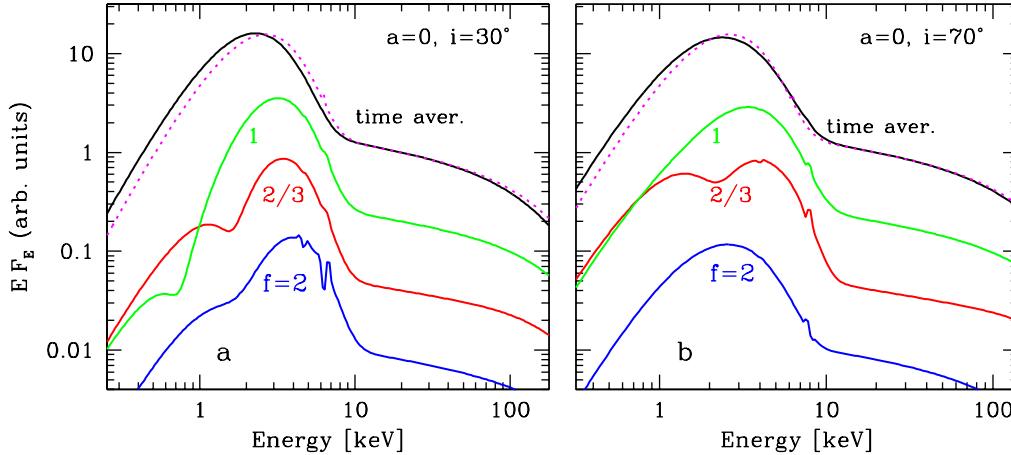


**Figure 6.** The QPO spectra for a non-rotating black hole case in the disc with corona geometry, for inclinations of  $i = 30^\circ$  (a) and  $i = 70^\circ$  (b). The curves are labeled as in Fig. 3.

Strength of the relativistic modulations depends also on the black hole spin. There is a dependence on  $a$  for a given radius, and, in the context of our models, there is also a dependence of  $r_{\text{QPO}}$  on  $a$ . We have therefore computed the QPO spectra for a non-rotating black hole,  $a = 0$ , in the disc-corona geometry, for two values of the inclination angle. Results are shown in Fig. 6. These show strong disc component, as expected from the geometry, broadened and/or shifted according to the variations of the extreme energy shifts.

Models computed above demonstrate that the QPO spectrum is generally similar to the spectrum emitted at the QPO radius. This is reasonable, since the relativistic effects simply smear out the emitted spectrum. Therefore, we also investigated a scenario, where the spectrum emitted at  $r_{\text{QPO}}$  is rather different than spectra emitted at neighboring radii. This is also motivated by results of modeling of many high luminosity states spectra, which reveal additional components. For example, often a very high state spectrum contains a disc thermal component and *two* Comptonized compo-

nents, one of which is from relatively cool optically thick plasma. Studies performed by, e.g., Done & Kubota (2006) suggest that such a cool Comptonized component may originate in inner part of accretion flow.

We have therefore assumed that the spectrum produced at  $r_{\text{QPO}}$  is a result of Comptonization of disc photons in a plasma of  $kT_e \approx 3$  keV and  $\tau_T = 7$ , while at other radii the parameters are as before. Results, for  $a = 0.998$  and  $i = 70^\circ$ , are presented in Fig. 7. The QPO spectra repeat the pattern observed also in Fig. 3 for the same  $a$  and  $i$ , in the sense that the  $f = 2$  QPO spectrum is broadest, and the  $f = 1$  and  $f = 2/3$  spectra are blueshifted.

## 5 DISCUSSION AND CONCLUSIONS

We have computed QPO energy spectra from the model assuming that the X-ray modulation is produced by variable relativistic effects from oscillating accretion flow. The model was suggested for

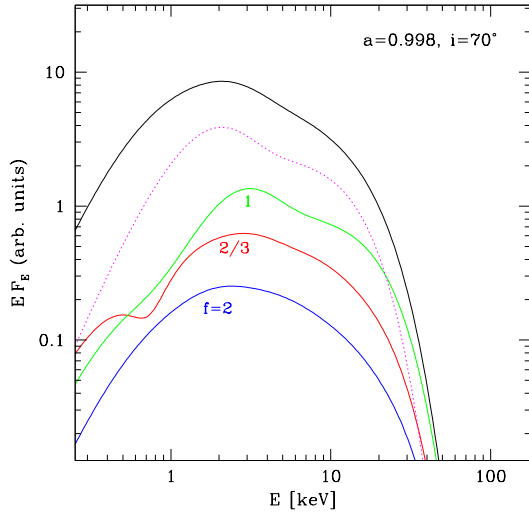


**Figure 7.** QPO spectra from a model, where the energy spectrum emitted at  $r_{\text{QPO}}$  is a Thomson thick low- $kT_e$  Comptonization (dotted curve, magenta online). The QPO spectra are similar to the spectrum emitted at  $r_{\text{QPO}}$ . Curves are labeled as in Fig. 3.

the high-frequency QPO observed in a number of black hole X-ray binaries, where pairs of QPO at frequencies with 3:2 ratio are often observed (Kluźniak & Abramowicz 2001). In its basic form the model assumes that the intrinsic luminosity of the X-ray source is constant (or at least there is no periodic component), and the entire observed modulation comes from the relativistic effects. This is currently the only model of high- $f$  QPO, which actually proposes a well defined mechanism of modulation of X-rays and thus can make predictions for spectral observables (see also Giannios & Spruit 2004 for a model of low- $f$  QPO).

Observations of hfQPO are rather difficult, but current data suggest that the thermal disc emission does not participate in the modulations (see review of observations in Sec. 2). It is however impossible to determine whether the QPO spectra are the same as the harder Comptonization component or they are systematically harder or softer than this. The former case would mean that the QPO might correspond to a simple modulation of luminosity of the Comptonization source, while the latter would imply either a dependence of spectral shape on radius, or spectral variability (e.g., Życki & Sobolewska 2005). The lack of modulation of the disc emission is, nevertheless, interesting since this appears to be a common property between the high- $f$  and low- $f$  QPO (Sobolewska & Życki 2006).

Our computations show that the proposed X-ray modulation mechanism produces QPO spectra which are qualitatively similar to the spectrum of emission from the QPO radius. Quantitatively, the QPO spectra are broadened and shifted under the influence of the Doppler and gravitational energy shifts. The amount of smearing depends on the extreme values of energy shifts, which themselves are functions of black hole spin (both directly and through the QPO radius, given by the resonance condition), and the inclination angle. Since the QPO energy spectra are really variability spectra, they depend also on the way  $g_{\text{min}}$  and  $g_{\text{max}}$  vary during the QPO cycle. This causes differences between spectra of different QPO.

In all our models where the disc thermal component is emitted at the QPO radius, it is variable and, obviously, it is present in

the QPO spectrum. If, however, the lack of the disc component is indeed a robust feature of the hfQPO spectra, it suggests (within the considered class of models) that the optically thick accretion disc is absent in the region of QPO generation, and only hot plasma is present. This would support a geometry with an inner hot torus, perhaps consistent with recent MHD simulations (e.g., Hawley & De Villiers, 2004 and references therein).

Energy dependencies of the two main QPO in the considered model are generally very similar, apart from the small differences discussed above. This might be a test of the model, if it turned out that the observed dependencies are different. For example, the pair of hfQPO in GRO J1655-40 seem to have different energy dependencies: the 450 Hz QPO has a hard spectrum (rms increasing with  $E$ ), while the 300 Hz seems to have a soft spectrum. The data are, however, not fully conclusive yet (Sec. 2).

## ACKNOWLEDGMENTS

This work was partly supported by grant no. 2P03D01225 from the Polish Ministry of Science and Higher Education.

## REFERENCES

- Abramowicz M. A., Karas V., Kluźniak W., Lee W. H., Rebusco P., 2003, *PASJ*, 55, 467
- Bardeen J. M., Press, W. H., Teukolsky, S. A., 1972, *ApJ*, 178, 347
- Belloni T., Soleri P., Casella P., Mendez M., Migliari, S., 2006, *MNRAS*, 369, 305
- Blaes O. M., Arras P., Fragile P. C., 2006, *MNRAS*, 369, 1235
- Bursa M., Abramowicz M. A., Karas V., Kluźniak W., 2004, *ApJ*, 617, L45
- Cui W., 1999, *ApJ*, 524, L59
- Cui W., Shrader C. R., Haswell C. A., Hynes R. I., 2000, *ApJ*, 535, L123
- Done C., Kubota A., 2006, *MNRAS*, 371, 1216
- Giannios, D.; Spruit, H. C. 2004, *A&A*, 427, 251
- Gierliński M., Done C., 2003, *MNRAS*, 342, 1083
- Hawley J. F., De Villiers J.-P., 2004, *PTHPS*, 155, 132
- Homan J., Wijnands R., van der Klis M., Belloni T., van Paradijs J., Klein-Wolt M., Fender R., Mendez M., 2001, *ApJS*, 132, 377
- Homan J., Klein-Wolt M., Rossi S., Miller J. M., Wijnands R., Belloni T., van der Klis M., Lewin W. H. G., 2003, *ApJ*, 586, 1262
- Homan J., Miller J. M., Wijnands R., van der Klis M., Belloni T., Steeghs D., Lewin W. H. G., 2005, *ApJ*, 623, 383
- Kalemcı E., Tomsick J. A., Rothschild R. E., Pottschmidt K., Kaaret P., 2001, *ApJ*, 563, 239
- Klein-Wolt M., Homan J., van der Klis M., 2004, *NuPhS*, 132, 381
- Kluźniak W., Abramowicz M. A., 2001, *AcPPB*, 32, 3605
- Krolik J. H., 1999, *Active Galactic Nuclei*, Princeton University Press, Princeton
- Lachowicz P., Czerny B., Abramowicz M., 2006, *MNRAS*, submitted, astro-ph/0607594
- Miller J. M. et al., 2001, *ApJ*, 563, 928
- Morgan E. H., Remillard R. A., Greiner J., 1997, *ApJ*, 482, 993
- Niedźwiecki A., 2005, *MNRAS*, 356, 913
- Remillard R. A., McClintock J. E., 2006, *ARA&A*, 44, 49
- Remillard R. A., McClintock J. E., Sobczak G. J., Bailyn C. D., Orosz J. A., Morgan E. H., Levine A. M., 1999a, *ApJ*, 517, L127
- Remillard R. A., Morgan E. H., McClintock J. E., Bailyn C. D., Orosz J. A., 1999b, *ApJ*, 522, 397
- Remillard R. A., Muno M. P., McClintock J. E., Orosz J. A., 2002, *ApJ*, 580, 1030
- Remillard R. A., McClintock J. E., Orosz J. A., Levine A. M., 2006, *ApJ*, 637, 1002
- Sobolewska M. A., Życki P. T., 2006, *MNRAS*, 370, 405
- Strohmayer T. E., 2001a, *ApJ*, 552, L49

Strohmayer T. E., 2001b, *ApJ*, 554, L169

Török G., Abramowicz M. A., Kluźniak W., Stuchlík Z., 2004, *A&A*, 436,

1

Zdziarski A. A., Johnson W. N., Magdziarz P., 1996, *MNRAS*, 283, 193

Życki P. T., 2003, *MNRAS*, 340, 639

Życki P. T., Niedźwiecki A., 2005, *MNRAS*, 359, 308

Życki P. T., Sobolewska M. A., 2005, *MNRAS*, 364, 891